Colossal negative thermal expansion induced by magnetic phase competition on frustrated lattices in Laves phase compound (Hf,Ta)Fe_{2}

B. Li, X. H. Luo, H. Wang, W. J. Ren, S. Yano, C.-W. Wang, J. S. Gardner, K.-D. Liss, P. Miao, S.-H. Lee, T. Kamiyama, R. Q. Wu, Y. Kawakita, and Z. D. Zhang

Phys. Rev. B **93**, 224405 — Published 6 June 2016

DOI: 10.1103/PhysRevB.93.224405

Colossal negative thermal expansion induced by magnetic phase competition on frustrated lattices in Laves phase compound (Hf,Ta)Fe_2

B. Li,[1,*] X. H. Luo,[2] H. Wang,[3] W. J. Ren,[2,†] S. Yano,[4] C.-W. Wang,[4] J. S. Gardner,[4] K.-D. Liss,[5] P. Miao,[6] S.-H. Lee,[6] T. Kamiyama,[6] R. Q. Wu,[3] Y. Kawakita,[1] and Z. D. Zhang[2]

[1] *Japan Proton Accelerator Research Complex (J-PARC), Japan Atomic Energy Agency, Tokai, Ibaraki 319-1195, Japan*

[2] *Shenyang National Laboratory for Material Sciences, Institute of Metal Research, Chinese Academy of Sciences, Shenyang 110016, China*

[3] *Department of Physics and Astronomy, University of California, Irvine, California 92697, USA*

[4] *Neutron Group, National Synchrotron Radiation Research Center, Hsinchu 30077, Taiwan*

[5] *Australian Nuclear Science and Technology Organisation (ANSTO), Lucas Heights, NSW 2234, Australia*

[6] *Neutron Science Laboratory, Institute of Materials Structure Science, High Energy Accelerator Research Organization (KEK), Tsukuba, Ibaraki 305-0801, Japan*

(Dated: May 20, 2016)

Competition between ferromagnetic and antiferromagnetic phases on frustrated lattices in hexagonal Laves phase compound $Hf_{0.86}Ta_{0.14}Fe_2$ is investigated by using neutron diffraction as a function of temperature and magnetic fields and density-functional-theory calculations. At 325 K, the compound orders into the 120° frustrated antiferromagnetic state with well-reduced magnetic moment and an in-plane lattice contraction simultaneously sets in. With further cooling down, however, the accumulated distortion in turn destabilizes this susceptible frustrated structure. The frustration is completely relieved at 255 K when the first-order transition to the ferromagnetic state takes place, where a colossal negative volumetric thermal expansion, -123×10^{-6}/K, is obtained. Meanwhile, the antiferromagnetic state can be suppressed by few Tesla magnetic fields, which results in a colossal positive magnetostriction. Such delicate competition is attributed to the giant magnetic fluctuation inherent in the frustrated antiferromagnetic state. Therefore, the magnetoelastic instability is approached even under a small perturbation.

PACS numbers: 81.05.Bx, 61.05.F-, 61.66.Fn, 75.30.-m

I. INTRODUCTION

The magnetic phase competition due to the comparable interactions dominates a wide variety of important magnetic phenomena[1,2]. The subtle compromise among individual phases gives rise to rich magnetic phase diagrams. In the vicinity of phase boundaries, moderate magnetic fields can induce a giant response, which is the origin of plenty of magnetic properties such as colossal magnetoresistance[1–4]. Magnetic frustration leading to high degeneracies usually promotes such competition and more intriguing magnetic behaviors are expected[5–7]. Taking the competition between ferromagnetic (FM) and antiferromagnetic (AFM) interactions as an example, the theoretical study suggests that a transition occurs from FM metal to paramagnetic (PM) metal on the geometrically frustrated pyrochlore lattice, rather than to AFM insulator in absence of the frustration effect[8]. Given that magnetic frustration is typically relieved to some extent via the lattice distortion[6,9], an interesting question how the lattice degree of freedom is influenced by this competition is raised. Peculiarly, negative thermal expansion (NTE) effects are sometimes accompanied by ordering of frustrated magnetic moments[10], such as in YMn_2[11,12], Mn_3(Gu,Ge)C[13], and $ZnCr_2Se_4$[14].

To this end, the magnetoelastic pseudo-binary Laves phase compounds $Hf_{1-x}Ta_xFe_2$, crystallizing in the geometrically frustrated hexagonal $MgZn_2$-type structure, probably are an ideal playground[15–18]. As shown in Fig. 1(a), it is a robust frustrated system in which Kagome-lattice layers formed by Fe ions occupying 6h sites and triangle-lattice layers of Fe ions located at 2a sites alternately repeat along the c direction. The intrinsic magnetism remains inconclusive, in spite of many attempts given in magnetization[15], ^{57}Fe Mössbauer spectra measurements[15,16] and neutron diffraction[17,18]. Note that no magnetic superlattice diffraction was observed in the neutron diffraction measurements. When $0.12 \leq x \leq 0.25$, two transitions successively take place as temperature decreases and the latter is accompanied by a NTE suggested by an earlier lab X-ray diffraction study[15]. Its large volumetric change is comparable with that of leading NTE materials nowadays[19].

To determine the magnetic structures and understand their coupling with the lattice, thus, we conducted a comprehensive study by combining high-resolution X-ray diffraction and neutron diffraction, and high-intensity neutron diffraction with complementary density-functional-theory (DFT) calculations. It is revealed that the colossal NTE with coefficient of volumetric thermal expansion as large as -123×10^{-6}/K is induced by the first-order magnetic transition from frustrated AFM to collinear FM states with the crystal symmetry preserved. Our study unambiguously indicates that magnetic frustration plays a crucial role in the NTE of this system and sheds light on searching of

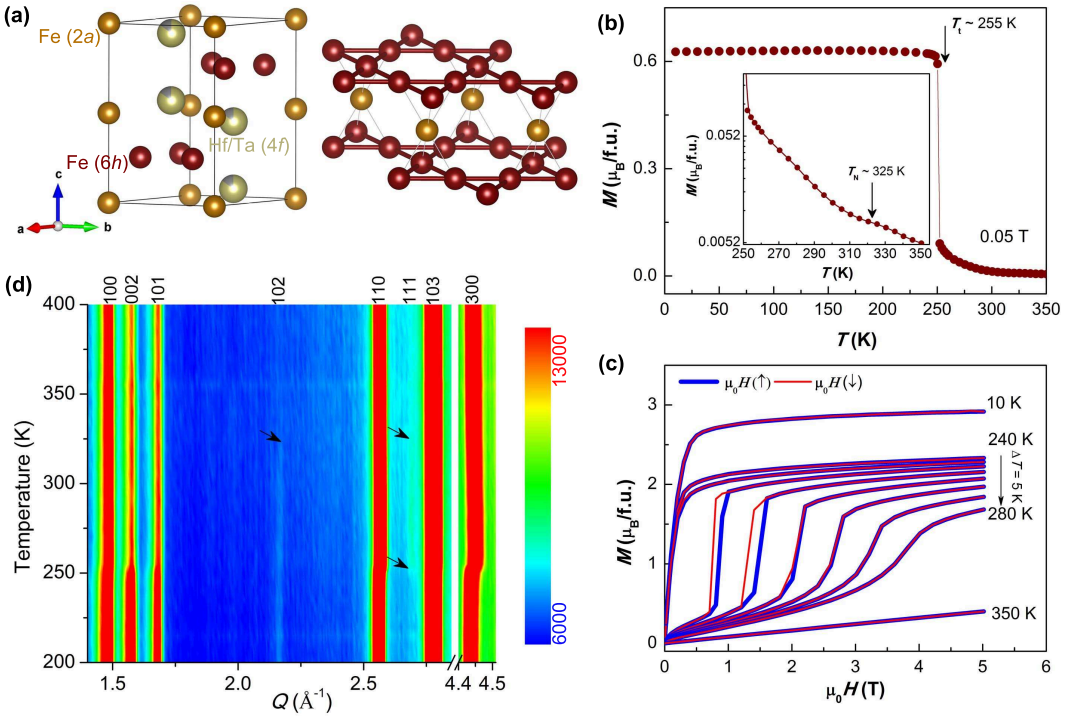

FIG. 1. (a) The crystal structure of $Hf_{1-x}Ta_xFe_2$. (b) The temperature dependence of magnetization per chemical formula. The inset shows the variation around 325 K. (c) The magnetic isotherms at selected temperatures with magnetic fields increasing and decreasing labeled by arrows. (d) The contour plot of neutron diffraction intensity. The feature temperatures are pointed out by the arrows.

NTE materials by tuning the competing magnetic orders on frustrated lattices.

II. EXPERIMENTS AND CALCULATIONS

The polycrystalline ingot was prepared by arc-melting the constituent elements with 99.9% purity. The temperature dependent high-resolution X-ray diffraction was carried out with Cu K_α radiation on a Rigaku SmartLab diffractometer equipped with a low temperature stage. Within the instrumental resolution of $\Delta d/d$ of 0.2-0.5%, there is no symmetry breaking identified[20]. The magnetization was measured by using Quantum Design MPMS XL. There are two transitions found at 325 and 255 K, which are labeled as T_N and T_t in Fig. 1(b), respectively. As shown in Fig. 1(c), the field dependence of magnetization appears as the typical FM behavior at 10 K while as a magnetic-field-induced transition with hysteresis between T_t and T_N. The neutron diffraction patterns with λ of 2.4 Å were collected at the high-intensity diffractometer Wombat with a 6 T magnet and at the high-resolution diffractometer Echidna of ANSTO[21,22]. Such combination allows us to thoroughly determine the structures. The diffraction data was analyzed by using the Rietveld refinement method in Fullprof[23]. SARAh[24] was utilized for the magnetic representational analysis. The composition was evaluated to be $Hf_{0.86}Ta_{0.14}Fe_2$ by the Rietveld refinement.

DFT simulations were performed with the Vienna Ab-initio Simulation Package (VASP)[25–28]. The spin-polarized generalized gradient approximation (GGA) was used for the description of the exchange-correlation interaction among electrons[29]. We treated Hf-5d6s, Ta-5d6s and Fe-3d4s as valence states and adopted the projector-augmented wave (PAW) pseudopotentials to represent the effect of their ionic cores[30,31]. To simulate the non-collinear AFM structure, the non-collinear magnetic mode was adopted with a negligible penalty contribution to the total energy adding into the Hamiltonian in order to keep the non-collinear local moment in the Kagome-lattice plane[32]. The energy cutoff for the plane-wave expansion was 500 eV, sufficient for transition metal compounds system according to our test calculations. Structures were optimized with a criterion that the atomic force on each atom became weaker than 0.01 eV/Å and the energy convergence is better than 10^{-6} eV.

III. RESULTS AND DISCUSSION

A. Neutron powder diffraction

In Fig. 1(d), we display the contour plot of diffraction intensity as a function of diffraction vector Q in the tem-

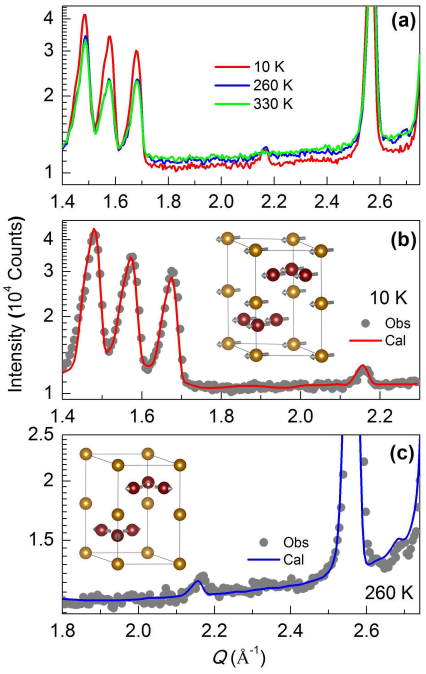

FIG. 2. (a) The neutron powder diffraction patterns at 10, 260 and 330 K. (b) and (c) The refinements of the data at 10 K (R_p = 4.01%, R_{wp} = 6.32%) and at 260 K (R_p = 5.98%, R_{wp} = 9.60%) with magnetic models that are shown as insets.

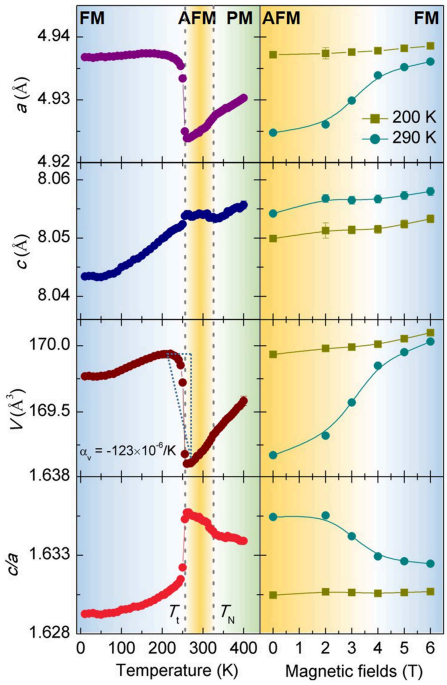

FIG. 3. The lattice constants a and c, volume V, and c/a of unit cell as functions of temperature (left) and of magnetic fields (right). The colorful shadows schematically illustrate the individual phase zones (AFM, FM, and PM) and their crossovers (only for 290 K in the right panel). The two dotted lines label T_N of 325 K and T_t of 255 K, respectively.

perature window from 200 to 400 K. The Bragg peaks are labeled with their Miller indices. With warming up, the intensity of the 002 peak drops dramatically at about 255 K, whereas the 300 peak exhibits a striking shift to higher Q. At the same time, a considerably weak peak suddenly sets in on the left of the 103 peak, which is identified as 111 peak. As temperature increases further, both 102 and 111 peaks vanish around 325 K. The significant enhancement of intensity of the 002 peak implies that magnetic moments lie in ab plane in the low-temperature phase. The presence of 111 peak in the intermediate phase indicates that this compound is most likely AFM because it is not crystallographically allowed in the space group of $P6_3/mmc$ and there is no crystal structural transition identified both in X-ray and neutron diffraction measurements down to 4 K. These variations are shown as well in Fig. 2(a) at selected temperatures. The feature temperatures above are well consistent with ones found in the temperature dependence of magnetization (Fig. 1(b)), respectively.

To completely determine the magnetic structures, we investigate the diffraction data at very low Q. The absence of superlattice diffraction peak suggests the propagation vector is (0,0,0). Thus, we carry out complete magnetic representational analysis of the space group $P6_3/mmc$ with this propagation vector. There are two FM arrangements allowed: one with moments pointing in the ab plane and another with moments along the c axis. The latter is excluded because the simulation with this model yields stronger magnetic intensity at positions of 100 and 101 peaks, which is distinct from the experimentally intense 002 magnetic peak[20]. However, the in-plane model is able to reproduce these features[20]. The refinement by including this in-plane magnetic model, without constraints on the moments at two sites, is shown in Fig. 2(b). The unfitted intensity around 1.4 Å might come from the tiny amount of impurity in our sample. The determined magnetic moments of Fe at 2a and 6h sites are pretty close and they are about 1.42(7) μ_B at 10 K and 1.16(7) μ_B at 240 K, respectively. They are converted to 2.84 and 2.32 μ_B for one chemical formula, well consistent with 2.9 and 2.3 μ_B found at 10 and 240 K under magnetic fields of 5 T in magnetization measurements, respectively. Note that 240 K is just few kelvins lower than T_t.

We turn our attention to the AFM state where the magnetic moments of Fe at 2a sites are disordered suggested by Mössbauer spectra measurements[16]. The diffraction patterns are compared at 260 and 330 K. First three Bragg peaks show nearly constant intensities. The identified differences are associated with 102 and 111 peaks, even though they are quite weak. In fact, the 111 peak is neither present in our high-resolution diffraction pattern taken at Echidna (not shown here), nor in previous neutron powder diffraction measurements with almost two orders of magnitude lower intensity[17,18]. The magnetic representational analysis provides two collinear

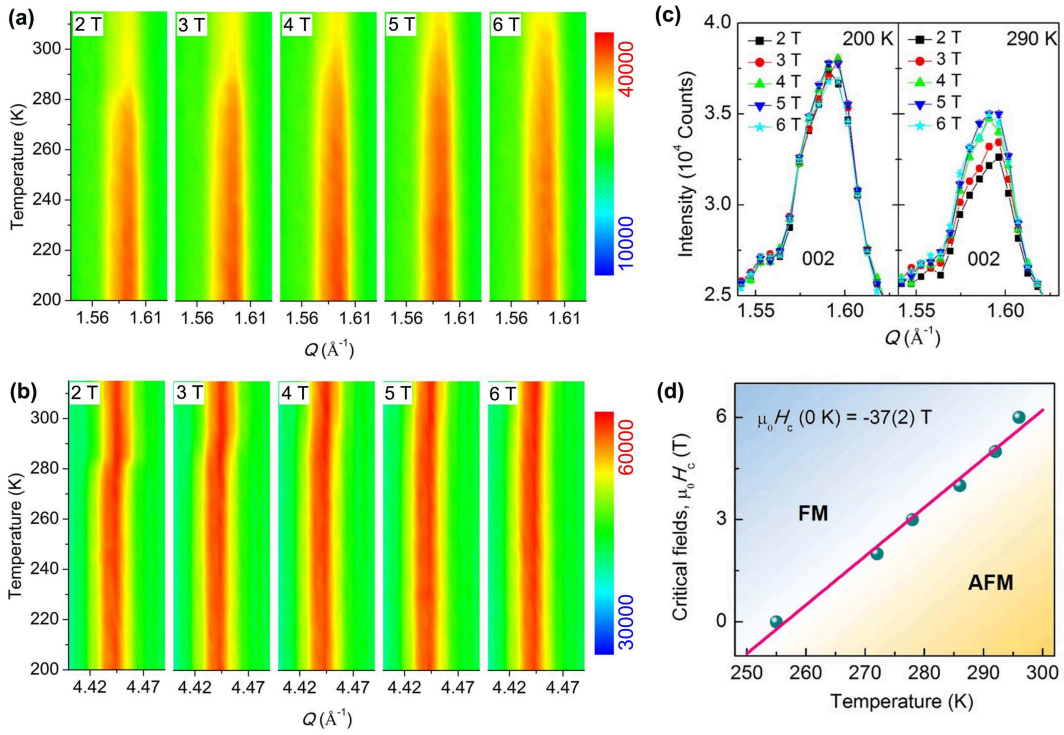

FIG. 4. (a) and (b) The contour plots of diffraction intensity of Bragg peaks 002 and 300 at different magnetic fields, respectively. (c) The Bragg peak 002 at 200 K (left) and at 290 K (right). (d) The phase diagram of the first-order transition. The phase boundary is well described by a linear relation with intercept of -37(2) T.

AFM structures in which the magnetic moments of Fe at the 6h sites either align along the c direction or lie in the ab plane, respectively. However, magnetic diffraction patterns generated for these two collinear models do not agree with experiments[20]. We hence need to consider frustrated AFM structures, where magnetic moments of Fe at the 6h sites form the 120° structure in the ab plane and interlayer coupling can be either FM or AFM. The 102 and 111 peaks can only be obtained for interlayer AFM configuration, and thus it is the most likely model for the AFM state in our system[20]. By taking the model, we refine the diffraction data, as shown in Fig. 2(c). The determined magnetic moment is around 0.6(1) μ_B. This is much smaller than 1.16(7) μ_B of the FM state at 240 K. Such AFM structure is actually the $q = 0$ Kagome AFM in the extended lattice as shown in the left panel of Fig. 1(a), differing from the $\sqrt{3} \times \sqrt{3}$ structure[33]. Moreover, the disordered moments of Fe at 2a sites sandwiched by two AFM coupled 6h layers might be frustrated as well. This would be the reason why the sizable moments of Fe at 2a sites are not ordered.

We summarize the temperature dependencies of lattice constants a and c, the volume V and the c/a ratio of unit cell in the left panel of Fig. 3. When temperature goes down through T_N of 325 K, the lattice shrinks in the ab plane rather than along the c direction. The temperature dependence of a obviously deviates from the linear relation for the PM state. This might be related to the exchange-striction effect arising from AFM ordering. At T_t of 255 K, a exhibits an large jump, $\Delta a/a$ about 0.3%, and the system transforms simultaneously to the FM state. Below T_t, a stays nearly constant while c gradually decreases. As shown by the slope triangle, V is increased by around 0.5% with varying temperature from 260 to 220 K, which is translated to a tremendous coefficient of volumetric thermal expansion, -123×10^{-6}/K. This value is in the same order of magnitude as -413×10^{-6}/K found in $Bi_{0.95}La_{0.05}NiO_3$ in the region of 300 - 360 K[34]. Meanwhile, c/a changes back to the ideal value $\sqrt{8/3}$ geometrically defined for the hexagonal closest packed structure after progressive increase below T_N.

The magnetic phase competition is examined in the magnetic fields and temperature phase-space by employing in-situ neutron diffraction. Typically, the contour plots of diffraction intensity of 002 and 300 Bragg peaks are shown in Fig. 4(a) and (b), respectively. The crossover of the intensity of the 002 peak, as an indication of AFM-FM transition, is prompted to higher temperatures with increasing magnetic fields. This means the AFM state is suppressed, in accordance with previous specific heat measured with magnetic fields[35] and our diffraction data under applied magnetic fields. At 200 K, it is FM so that the intensity is much less susceptible to magnetic fields than at 290 K where it is AFM. The intensity at 290 K becomes almost field independent beyond 4 T, which roughly defines the critical field inducing

TABLE I. Comparison of lattice dimensions from experiments and the DFT calculations for three magnetic states. The first row is for calculated values while the second one is for experimental values at selected temperatures. The calculations are based on the $2a \times a \times c$ supercell.

States	E (eV)	a (Å)	c (Å)	V (Å^3)	c/a	M_{2a} (μ_B)	M_{6h} (μ_B)
PM	-220.491	4.812	7.980	320.02	1.658	0	0
	(400 K)	4.9303(4)	8.0557(7)	169.583(35)	1.6339	0	0
FM	-222.119	4.917	7.988	335.51	1.625	1.75	1.76
	(10 K)	4.9368(4)	8.0434(5)	169.770(9)	1.6293	1.42(7)	1.42(7)
AFM	-220.57	4.843	7.988	324.51	1.649	0.2	1.19
	(260 K)	4.9239(4)	8.0541(4)	169.108(8)	1.6357	0	0.6(1)

the AFM to FM transition. In response to the applied magnetic fields, the lattice is concomitantly expanded in the ab plane, as seen in the shift of the 300 peak. The detailed field dependencies of lattice dimensions are compared with their temperature dependencies in Fig. 3. The diffraction under in-situ magnetic fields enables us to directly determine the magnetic phase diagram. The transition temperature is defined as one where the lattice constant a of the FM state starts to sharply drop. There is a linear relationship as depicted by the fitting shown in Fig. 4(d), similar with the other systems with AFM-FM transitions[36]. The intercept represents the extrapolated critical fields for the AFM to FM transition at 0 K.

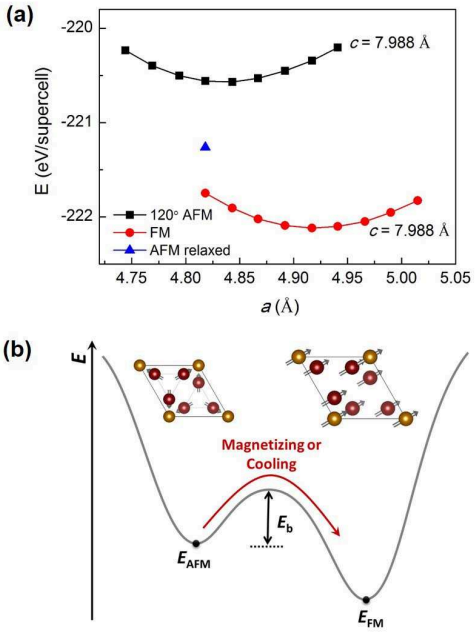

FIG. 5. (a) Total energy calculation of frustrated AFM state and FM state. c is fixed at 7.988 Å that is the value for the FM state in a fully relaxed calculation. (b) The schematic diagram of ground state energy landscape of the first-order transition from AFM to FM states with magnetizing or cooling, whose structures are shown along c direction.

B. DFT calculations

The reentrant temperature dependence of c/a in the vicinity of AFM phase reflects the magnetic phase competition and suggests the existence of an energy minimum in the energy profile with respect to the lattice dimensions, which is justified by our DFT total energy calculation on a $2a \times a \times c$ supercell (Hf_7TaFe_{16}). This adopted supercell is the smallest one whose composition, $Hf_{0.875}Ta_{0.125}Fe_2$, can match the actual one. We consider three magnetic configurations: FM, 120° AFM, and PM. The FM ordering significantly lowers the total energy and expands the lattice compared with the PM state, as listed in Table I. Then, the variation of total energy in the AFM configuration is examined by the calculation with varying lattice constant a when c is fixed at the FM value of 7.988 Å. It can be seen in Fig. 5(a) that the AFM arrangement prefers the in-plane contraction as reflected at the reduced total energy when a is decreased from that of FM. However, the system is destabilized by a further compression after passing through the energy minimum. It is consequently concluded that the lattice distortion energy most likely governs the phase competition. The local energy minimum of FM state is exactly determined by the DFT calculation to be -222.119 eV for the supercell. In the AFM state, a symmetry-breaking of the lattice is found in the fully relaxed calculation. The resulted total energy, -221.263 eV (triangle in Fig. 5(a)), provides the lower bound of the total energy in the frame of DFT.

C. Relevance to NTE

The delicate magnetic phase competition is facilitated by the magnetic frustration that manifests itself as unique energy landscape schematically drawn in Fig. 5(b). Two local energy minima correspond to FM and AFM states whose structures along the c direction are shown on the top, respectively. The AFM one is less stable due to the frustration effect. They are separated by an energy barrier (E_b), which is measured by magnetic Zeeman energy exerted by critical fields $\mu_0 H_c(0\ \mathrm{K})$. It is estimated to be about 6 meV per chemical formula.

At finite temperatures, E_b is significantly reduced by the giant magnetic fluctuation. Accordingly, this transition can be activated by a small perturbation like decreasing temperature (leading to *self-compression* due to AFM exchange-striction) or applying moderate magnetic fields. It is this energy profile that the colossal NTE effect comes up.

The fluctuating nature of the AFM state is well supported by the thermodynamic measurements. On one hand, it is evidenced by the magnetocaloric and barocaloric effects. The entropy change at the magnetic-field-induced AFM to FM transition is negative[37] while it is positive at pressure-induced FM to AFM transition inferred by volumetric Clausius-Clapeyron relation with dT_t/dP = -130 K/GPa[38,39]. The Debye temperature is almost composition independent when x is changed from 0 to 0.5 in $Hf_{1-x}Ta_xFe_2$, which correspond to FM and AFM ground states, respectively, so that the observed entropy changes mostly originate from the magnetic subsystem[40]. They are clearly indicative of stronger disorder in the AFM state. On another hand, the electronic specific heat coefficient γ of the AFM state in $Hf_{1-x}Ta_xFe_2$ also suggests the giant spin fluctuation. It is determined to be 40 mJ/K^2, nearly twice larger than that of the FM state (about 20 mJ/K^2) as well as that of the crystallographically isostructural but magnetically non-frustrated AFM $TiFe_2$ (22 mJ/K^2)[41,42]. This discrepancy might be attributed to the magnetic frustration. In highly frustrated (Y,Sc)Mn_2, similarly, an enormously large γ, 150 mJ/K^2, is observed[12].

IV. SUMMARY

To summarize, the complete crystal and magnetic structures of $Hf_{0.86}Ta_{0.14}Fe_2$ are determined by using neutron powder diffraction. The magnetic phase competition, enabled by the magnetic frustration, is well demonstrated in $\mu_0 H - T$ phase-space. The lattice distortion is revealed to dominate the magnetic phase competition as seen in the reentrant behavior of c/a, supported by DFT calculations. The interplay of the FM, AFM interactions with the lattice distortion leads to the colossal volumetric variations of unit cell in response to the changes of temperature and magnetic field. This suggests that tailoring competing magnetic phases on frustrated lattices is an effective route to NTE and it is worthwhile to extend such scenario to other related compounds.

ACKNOWLEDGMENTS

The authors acknowledge the merit award of instrument time at the OPAL reactor of ANSTO. X. H. Luo, W. J. Ren and Z. D. Zhang were supported by the National Natural Science Foundation of China (Grant No. 51331006 and 51531008). Work at UCI was supported by DOE-BES (Grant No. DE-FG02-05ER46237). Computer simulations were performed at the U.S. Department of Energy Supercomputer Facility (NERSC).

* bing.li@j-parc.jp
† wjren@imr.ac.cn

[1] M. Imada, A. Fujimori, and Y. Tokura, *Rev. Mod. Phys.* **70**, 1039 (1998).
[2] E. Dagotto, *Science* **309**, 257 (2005).
[3] K. A. Gschneidner Jr.,V. K. Pecharsky and A. O. Tsokol, *Rep. Prog. Phys.* **68**, 1479 (2005).
[4] S. B. Roy, *J. Phys.: Condens. Matter* **25**, 183201 (2013).
[5] L. Balents, *Nature* **464**, 199 (2010).
[6] C. Lacroix, P. Mendels, and F. Mila, Introduction to Frustrated Magnetism: Materials, Experiments, Theory (Springer, New York, 2011).
[7] J. S. Gardner, M. J. P. Gingras, and J. E. Greedan, *Rev. Mod. Phys.* **82**, 53107 (2010).
[8] Y. Motome and N. Furukawa, *Phys. Rev. Lett.***104**, 106407 (2010).
[9] S.-H. Lee et al., *J. Phys. Soc. Jpn.* **79**, 011004 (2010).
[10] A. P. Ramirez, C. L. Broholm, R. J. Cava, and G. R. Kowach, *Physica B* **280**, 290 (2000).
[11] Y. Nakamura, *J. Magn. Magn. Mater.* **31-34** (1983) 829.
[12] M. Shiga, K. Fujisawa, and H. Wada, *J. Phys. Soc. Jpn.* **62**, 1329 (1993).
[13] K. Takenaka and H. Takagi, *Appl. Phys. Lett.* **87**, 261902 (2005).
[14] J. Hemberger, H.-A. Krug von Nidda, V. Tsurkan, and A. Loidl, *Phys. Rev. Lett.***98**, 147203 (2007).
[15] Y. Nishihara and Y. Yamaguchi, *J. Phys. Soc. Jpn.* **52**, 3630 (1983).
[16] H. R. Rechenberg, L. Morellon, P. A. Algarabel, and M. R. Ibarra, *Phys. Rev. B* **71**, 104412 (2005).
[17] H. G. M. Duijn et al., *J. Appl. Phys.* **81**, 4218 (1997).
[18] L. V. Diop, O. Isnard, E. Suard and D. Benea, *Solid State Commun.* **229**, 16 (2016).
[19] J. Chen, L. Hu, J.-X. Deng, and X.-R. Xing, *Chem. Soc. Rev.* **44**, 3522 (2015).
[20] See Supplemental Material at [URL will be inserted by publisher] for X-ray diffraction patterns and simulated magnetic diffraction patterns with different FM and AFM models.
[21] A. J. Studer, M. E. Hagen, and T. J. Noakes, *Physica B* **385-386**, 1013 (2006).
[22] K.-D. Liss, B. Hunter, M. Hagen, T. Noakes, and S. Kennedy, *Physica B* **385-386**, 1010 (2006).
[23] J. Rodriguez-Carvajal, *Physica B* **192**, 55 (1993).
[24] A. S. Wills, *Physica B* **276-278**, 680 (2000).
[25] G. Kresse and J. Furthmuller, *Phys. Rev. B* **54**, 11169 (1996).
[26] G. Kresse and J. Hafner, *Phys. Rev. B* **49**, 14251 (1994).
[27] G. Kresse and J. Hafner, *Phys. Rev. B* **47**, 558 (1993).
[28] G. Kresse and J. Furthmuller, *Comput. Mater. Sci.* **6**, 15 (1996).
[29] J. P. Perdew, K. Burke, and M. Ernzerhof, *Phys. Rev. Lett.* **77**, 3865 (1996).

[30] G. Kresse and D. Joubert, *Phys. Rev. B* **59**, 1758 (1999).
[31] P. E. Blöchl, *Phys. Rev. B* **50**, 17953 (1994).
[32] P.-W. Ma and S. L. Dudarev, *Phys. Rev. B* **91**, 054420 (2015).
[33] A. Chubukov, *Phys. Rev. Lett.* **69**, 832 (1992).
[34] M. Azuma et al., *Nat. Commun.* **2**, 347 (2011).
[35] P. Bag, R. Rawat, P. Chaddah, P. D. Babu, and V. Siruguri, *Phys. Rev. B* **93**, 014416 (2016).
[36] B. Li et al., *Appl. Phys. Lett.* **100**, 242408 (2012);
[37] Z. Han et al., *J. Alloys Comp.* **377**, 75 (2004).
[38] L. Morellon, P. A. Algarabel, M. R. Ibarra, Z. Arnold, and J. Kamard, *J. Appl. Phys.* **80**, 6911 (1996).
[39] D. Matsunami, A. Fujita, K. Takenaka, and M. Kano, *Nat. Mater.* **14**, 73 (2015).
[40] H. Wada, N. Shimamura, and M. Shiga, *Phys. Rev. B* **48**, 10221 (1993).
[41] P. J. Brown, J. Deportes, and B. Ouladdiaf, *J. Phys.: Condens. Matter* **4**, 10015 (1992).
[42] H. Wada, M. Hada, M. Shiga, and Y. Nakamura, *J. Phys. Soc. Jpn.* **59**, 701 (1990).